Hindawi
International Journal of Antennas and Propagation
Volume 2020, Article ID 3952175, 11 pages
https://doi.org/10.1155/2020/3952175

Research Article

A Novel Method for DOA and Time Delay Joint Estimation in Multipath OFDM Environment

Xiangzhi Li, Weijia Cui, Haiyun Xu, Bin Ba, and Yankui Zhang

National Digital Switching System Engineering & Technological Research Center, Zhengzhou 450001, China

Correspondence should be addressed to Bin Ba; xidianbabin@163.com

Received 2 September 2019; Revised 5 December 2019; Accepted 20 December 2019; Published 30 January 2020

Academic Editor: Giuseppe Castaldi

Joint time delay and direction of arrival estimation based on uniform linear arrays in Orthogonal Frequency Division Multiplexing (OFDM) systems has to face the problems posed by coherent multipath environments and high computational complexity. In this paper, a novel fast method is proposed to achieve a joint direction-of-arrival (DOA) and time-dealy (TD) estimation of multipath OFDM signals by fully using space-frequency characteristics. Firstly, we construct an extended virtual array by combining the array structure and frequency-domain information. Then, we calculate the extended channel frequency response matrix and adopt smoothing processing to eliminate the multipath effect. Next, we get the result of DOA estimation by using a closed-form solution, which costs little complexity and can achieve fast estimation. Finally, we conduct a one-dimensional spectral search using the obtained DOA values to estimate time delays. Simulation results show that our proposed methods have excellent performance even under low SNR conditions in different multipath environments. Furthermore, methods proposed in this paper have much less computational complexity and better estimation performance compared with the multidimensional spectral peak search methods.

1. Introduction

The technology of Orthogonal Frequency Division Multiplexing (OFDM) is one of the Multi-Carrier Modulation (MCM) technologies with low implementation complexity and high bandwidth efficiency [1]. Due to the multicarriers, one of OFDM's advantages is that it can combat frequency-selective fading and narrowband interference, ensuring its application in high-speed data transmission fields [2]. Now, OFDM has been widely applied in IEEE 802.11 wireless local area network, the next generation mobile communication, and digital video broadcasting (DVB) [3–5]. In addition to data service, OFDM systems also provide users with location-based service.

Time delay (TD) and direction of arrival (DOA) are two main parameters of location-based scenarios, such as radar and mobile communication [6]. Researchers have proposed various super-resolution algorithms for parameter estimation. The multiple signal classification (MUSIC) algorithm for time delay estimation based on narrowband signals is proposed in [7]. Reference [8] presents a propagator method (PM) for time delay estimation. Estimating signal parameters via rotational invariance techniques (ESPRIT) is proposed in [9] in order to reduce the high complexity of 2D search. References [10, 11] use the compressive sensing method to conduct the estimation in underdetermined conditions. When it comes to DOA estimation, the multiple signal classification (MUSIC) algorithm [12] and root-MUSIC [13] have been developed and widely used. The researchers of [14] propose a space-time conversion MUSIC (STC-MUSIC) algorithm for DOA estimation. However, the abovementioned algorithms are only applicable for narrowband signals, so the estimation accuracy of these algorithms are less improved due to the limitation of frequency bandwidth and array aperture.

Based on OFDM signals, many methods have also been proposed for joint estimation of time delay and DOA. Reference [13] presents a method for joint estimation based on root-MUSIC; authors of [15] apply the space-alternating generalized expectation-maximization (SAGE) algorithm for the joint estimation of time delay and DOA; [16] develops a method achieving joint estimation of DOA and time

delay based on frequency-domain processing with a two-antenna receiver; for 3D massive MIMO-OFDM systems, joint estimation methods are introduced based on parametric channel modeling [17, 18]; but all these algorithms cannot be applied in multipath environments when received signals are coherent of each other, which result in signal distortion and estimation error [19]. Besides, some researchers have proposed algorithms using frequency subcarriers as a way to extend virtual aperture [20]. One method is to construct an extended channel frequency response matrix using Hadamard product [21]. Another method is introduced in [22] that can achieve joint estimation by using a 2D active broadband MIMO-OFDM system, which requires a large number of antennas. Furthermore, [23] needs only three antennas to achieve joint DOA and TOA estimation based on multidimensional peak searching. The abovementioned methods can achieve high precision, but the computational complexity is too high.

Multipath is common in wireless communication which will result in the signals reaching the aerials through two or more paths. Multipath effect would cause multipath fading, and there would be interference between different paths [24]. Meanwhile, the estimation of time delay and DOA of each path is required in location determination, high-precision measurement, and UAV tracking [25].

As can be seen, most of the previous researches focus mainly on independent multipath environment where subspace algorithms can be used to estimate DOA. But they are not applied to coherent signals. When the multipaths are coherent, spatial smoothing processing can be a solution, but it will lead to the loss of array aperture [26]. Reference [27] introduces an indoor passive localization called eigenspace-based DOA with direct-path recognition (ES-DPR). Meanwhile, the computational complexity is too high when spectrum searching methods are applied [28].

As a result, we propose a method that can achieve both high-precision and fast joint estimation with a low complexity in both independent and coherent multipath environments based on OFDM signals that can be applied in ULA. We first extend the array aperture by constructing the extended channel frequency response which contains all subcarrier information and array information. The extended matrix is used to estimate DOA and time delay as they are included in the matrix. Next, when dealing with coherent signals, we use the virtue smoothing method by dividing the extended manifold matrix into submatrices on the basis of multiple subcarriers and also prove that the average of the submatrices is nonsingular, meaning that subspace-based methods could be applied for joint estimation. Then, we use the TLS-ESPRIT method for a closed-form solution to reduce computational complexity. Lastly, simulation results show the high accuracy and efficiency compared with separate estimation methods and the spectral peak searching method.

The main contribution of this paper is utilizing space-frequency characteristics of OFDM signals to deal with the estimation problem in multipath environment. The signal model introduced in this paper considers both space domain and frequency domain, which ensures the expansion of array aperture. Besides, the virtual spatial smoothing in this paper is quite different from traditional ones. It is conducted in the frequency domain, and there is no loss of array aperture. Consequently, the performance of our joint estimation method is better than that of the super-resolution methods.

The paper is organized as follows. Chapter 2 introduces the signal model used in this paper. Chapter 3 describes our proposed method for joint estimation of DOA and time delay in detail. Then, the computational complexity is calculated and compared in Chapter 4. Chapter 5 presents simulation results to verify the performance of the proposed method.

Notations. In this paper, $(\bullet)^{\mathrm{H}}$ represents the conjugate transpose, $E[\bullet]$ represents the expectation value, and $\mathrm{diag}(\bullet)$ denotes the transformation of a vector into a diagonal matrix.

2. Signal Model

A uniform linear array (ULA) is adopted in this paper, which is composed of M sensors. Suppose the signals are all far-field, which ensure the wave-fronts arriving at the sensors are plane waves. The received signal model is shown in Figure 1. In this paper, θ_p is defined as the angle between the normal direction of the array and the straight ray. The reference sensor is numbered as 1, and τ_p is the propagation delay of the p-th path from the emission source to the reference sensor. The relative delay of the p-th path between the reference sensor and the m-th sensor is represented as

$$\xi_{p,m} = \frac{(m-1)d \sin \theta_p}{c}, \tag{1}$$

where d represents the distance between two adjacent elements, which is half-wavelength of incident signals; and c is the speed of light.

The multipath radio propagation channel is generally modeled as a complex low-pass equivalent impulse response. The response of m-th sensor in n-th time interval could be represented as

$$h_m^{(n)}(t) = \sum_{p=1}^{P} \alpha_p^{(n)} e^{j\beta_p^{(n)}} \delta^{(n)}\left(t - \tau_p - \xi_{p,m}\right), \tag{2}$$

where P is the multipath number. $\alpha_p^{(n)} e^{j\beta_p^{(n)}}$ is the complex attenuation of p-th path, α_p is the amplitude, and β_p is the phase with a uniform distribution represented as $\beta_p \sim U(0, 2\pi)$.

Suppose there are L subcarriers in the OFDM system. Based on Fourier transformation, the channel frequency response of the m-th sensor with the l-th subcarrier could be represented as

$$H_{l,m}^{(n)} = \sum_{p=1}^{P} \alpha_p^{(n)} e^{j\beta_p^{(n)}} e^{-j2\pi\left(f_c + l\Delta f\right)\left(\tau_p + \xi_{p,m}\right)} + n_{l,m}^{(n)}, \tag{3}$$

where f_c is the carrier frequency, Δf is the OFDM subcarrier spacing, and $n_{l,m}^{(n)} \sim N(0, \sigma^2)$ is additive white

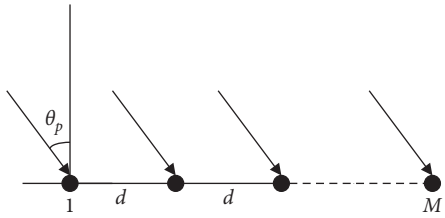

Figure 1: Signal arrival to uniform linear array.

Gaussian noise. So, the channel frequency response of the l-th subcarrier is

$$\mathbf{H}_l^{(n)} = \mathbf{A}_l(\boldsymbol{\tau}, \boldsymbol{\xi})\mathbf{b}^{(n)} + \mathbf{n}_l^{(n)}, \tag{4}$$

or

$$\mathbf{H}_l^{(n)} = \mathbf{A}_l(\boldsymbol{\tau}, \boldsymbol{\theta})\mathbf{b}^{(n)} + \mathbf{n}_l^{(n)}, \tag{5}$$

where

$$\begin{aligned} \boldsymbol{\tau} &= [\ \tau_1 \ \ \tau_2 \ \ \dots \ \ \tau_P\ ], \\ \boldsymbol{\xi}_p &= [\ \xi_{p,1} \ \ \xi_{p,2} \ \ \dots \ \ \xi_{p,M}\ ]^T, \quad p = 1, 2, \dots, P, \\ \boldsymbol{\xi} &= [\ \xi_1 \ \ \xi_2 \ \ \dots \ \ \xi_P\ ], \\ \boldsymbol{\theta} &= [\ \theta_1 \ \ \theta_2 \ \ \dots \ \ \theta_P\ ]. \end{aligned} \tag{6}$$

Then, we define

$$\mathbf{A}_l(\boldsymbol{\tau}, \boldsymbol{\xi}) = [\ a_l(\tau_1, \xi_1) \ \ a_l(\tau_2, \xi_2) \ \ \dots \ \ a_l(\tau_P, \xi_P)\ ], \tag{7}$$

$$\mathbf{a}_l(\boldsymbol{\tau}_p, \boldsymbol{\xi}_p) = [\ a_l(\tau_p, \xi_{p,1}) \ \ a_l(\tau_p, \xi_{p,2}) \ \ \dots \ \ a_l(\tau_p, \xi_{p,M})\ ]^{\mathrm{T}}, \tag{8}$$

where $a_l(\tau_p, \xi_m) = e^{-j2\pi(f_c + l\Delta f)(\tau_p + \xi_{p,m})}$, and

$$\begin{aligned} \mathbf{b}^{(n)} &= [\ \alpha_1^{(n)} e^{j\beta_1^{(n)}} \ \ \alpha_2^{(n)} e^{j\beta_2^{(n)}} \ \ \dots \ \ \alpha_P^{(n)} e^{j\beta_P^{(n)}}\ ]^T, \\ \mathbf{n}_l^{(n)} &= [\ n_{l,1}^{(n)} \ \ n_{l,2}^{(n)} \ \ \dots \ \ n_{l,M}^{(n)}\ ]^T. \end{aligned} \tag{9}$$

Suppose there are N time intervals when receiving the multipath signals; as a result, (4) is reformulated into

$$\mathbf{H}_l = \mathbf{A}_l(\boldsymbol{\tau}, \boldsymbol{\xi})\mathbf{B} + \mathbf{n}_l, \tag{10}$$

where

$$\begin{aligned} \mathbf{B} &= [\ \mathbf{b}^{(1)} \ \ \mathbf{b}^{(2)} \ \ \dots \ \ \mathbf{b}^{(N)}\ ], \\ \mathbf{n}_l &= [\ \mathbf{n}_l^{(1)} \ \ \mathbf{n}_l^{(2)} \ \ \dots \ \ \mathbf{n}_l^{(N)}\ ]. \end{aligned} \tag{11}$$

According to the abovementioned formulas, the extended channel frequency-domain response could be constructed by arranging the L channel frequency-domain responses, represented as

$$\mathbf{H} = \begin{bmatrix} \mathbf{H}_0 \\ \mathbf{H}_1 \\ \vdots \\ \mathbf{H}_{L-1} \end{bmatrix} = \begin{bmatrix} \mathbf{A}_0(\boldsymbol{\tau}, \boldsymbol{\xi}) \\ \mathbf{A}_1(\boldsymbol{\tau}, \boldsymbol{\xi}) \\ \vdots \\ \mathbf{A}_{L-1}(\boldsymbol{\tau}, \boldsymbol{\xi}) \end{bmatrix} \mathbf{B} + \begin{bmatrix} \mathbf{n}_0 \\ \mathbf{n}_1 \\ \vdots \\ \mathbf{n}_{L-1} \end{bmatrix} = \mathbf{A}(\boldsymbol{\tau}, \boldsymbol{\xi})\mathbf{B} + \mathbf{n}. \tag{12}$$

The uniformly distributed subcarriers have something similar to the array sensors of the ULA in the channel frequency-domain response, which is called space-time equivalence. By constructing the extended frequency-domain response, the dimension of virtual bandwidth is expanded by M time from L to ML. Similarly, the array aperture is expanded by $(ML-1)/(M-1)$ times. As is deduced above, the original aperture is $M-1$, and finally the virtual aperture is $ML-1$. According to the previous analysis and theory, the expanded bandwidth and array aperture could greatly improve the estimation performance of signal parameters.

3. Joint DOA and Time Delay Estimation

The covariance matrix of $\mathbf{H}$ could be represented as

$$\mathbf{R}_{\mathrm{H}} = E\left[\mathbf{H}\mathbf{H}^{\mathrm{H}}\right] = \frac{1}{N}\mathbf{H}\mathbf{H}^{\mathrm{H}} = \mathbf{A}(\boldsymbol{\tau}, \boldsymbol{\xi})\mathbf{R}_{\mathrm{B}}\mathbf{A}^{\mathrm{H}}(\boldsymbol{\tau}, \boldsymbol{\xi}) + \sigma^2\mathbf{I}. \tag{13}$$

In formula (12), $\mathbf{R}_{\mathrm{B}}$ is the covariance matrix of complex attenuation matrix $\mathbf{B}$. When the complex attenuations $\alpha_p^{(n)} e^{j\beta_p^{(n)}}$, $p = 1, 2, \dots, P$ are independent from each other at every sampling time, it would be clear that $\mathrm{rank}(\mathbf{R}_{\mathrm{B}}) = P$. Besides, $\mathbf{A}(\boldsymbol{\tau}, \boldsymbol{\xi})$ is of full column rank and $\mathrm{rank}(\mathbf{A}(\boldsymbol{\tau}, \boldsymbol{\xi})) = P$, so we can get that $\mathrm{rank}(\mathbf{A}(\boldsymbol{\tau}, \boldsymbol{\xi})\mathbf{R}_{\mathrm{B}}\mathbf{A}^{\mathbf{H}}(\boldsymbol{\tau}, \boldsymbol{\xi})) = P$. Under this condition, the MUSIC algorithm could be adopted to estimate the parameters. First, we can get noise subspace $\mathbf{U}_N$ through eigenvalue decomposition of matrix $\mathbf{R}_{\mathrm{H}}$. According to the relationship between $\mathbf{U}_N$ and $\mathbf{A}(\boldsymbol{\tau}_p, \boldsymbol{\xi}_p)$,

$$\mathbf{A}^{\mathrm{H}}(\boldsymbol{\tau}_p, \boldsymbol{\xi}_p)\mathbf{U}_N = 0, \quad p = 1, 2, \dots, P. \tag{14}$$

Then, the spatial spectrum function could be constructed as

$$P(\boldsymbol{\tau}, \boldsymbol{\theta}) = \frac{1}{\mathbf{A}^{\mathrm{H}}(\boldsymbol{\tau}, \boldsymbol{\theta})\mathbf{U}_N\mathbf{U}_N^{\mathrm{H}}\mathbf{A}(\boldsymbol{\tau}, \boldsymbol{\theta})}. \tag{15}$$

The estimated values $(\boldsymbol{\tau}_p, \boldsymbol{\theta}_p)$ would be located in the peaks of $P(\boldsymbol{\tau}, \boldsymbol{\theta})$. However, the computational complexity of MUSIC based on the extended channel frequency-domain response (EX-MUSIC) is too high to be practical in actual applications. Furthermore, the premise of using MUSIC that $\mathrm{rank}(\mathbf{R}_{\mathrm{B}}) = P$ fails, because in the multipath environment, the complex attenuations are coherent with each other, and therefore $\mathrm{rank}(\mathbf{R}_{\mathrm{B}}) < P$, $\mathrm{rank}(\mathbf{A}(\boldsymbol{\tau}, \boldsymbol{\xi})\mathbf{R}_{\mathrm{B}}\mathbf{A}^{\mathbf{H}}(\boldsymbol{\tau}, \boldsymbol{\xi})) < P$.

Consequently, new methods are needed in complex multipath environment.

3.1. The Smoothing Preprocessing. Smoothing processing is one of the effective methods used to solve the parameter estimation problem of coherent signals. The traditional spatial smoothing works by dividing the ULA into several sub-arrays, which would severely limit the maximum number of signals the array can estimate. On the basis of expanding virtual aperture, we therefore propose a new virtual smoothing method without losing the degree of freedom (DOF).

We divide the extended virtual array with manifold matrix $\mathbf{A}(\boldsymbol{\tau}, \boldsymbol{\xi})$ into L virtual subarrays, whose manifold matrices are $\mathbf{A}_l(\boldsymbol{\tau}, \boldsymbol{\xi})$, $l = 0, 1, \ldots, L-1$. That is to say, the l-th virtual subarray contains the l-th subcarrier of each sensor, and $1 \le l \le L$.

As is introduced in [28], the next step is to define the covariance matrix of each subarrays. The frequency-domain response of $\mathbf{A}_l(\boldsymbol{\tau}, \boldsymbol{\xi})$ is $\mathbf{H}_l$, $l = 0, 1, \ldots, L-1$, and the covariance matrix could be represented as

$$\mathbf{R}_{\mathrm{H}_l} = \frac{1}{N}\mathbf{H}_l\mathbf{H}_l^{\mathrm{H}} = \mathbf{A}_l(\boldsymbol{\tau}, \boldsymbol{\xi})\mathbf{R}_{\mathrm{B}}\mathbf{A}_l^{\mathrm{H}}(\boldsymbol{\tau}, \boldsymbol{\xi}) + \sigma^2\mathbf{I}. \tag{16}$$

When describing the signal model, it is assumed that signals are far enough from the ULA. As a result, the relative delay $\boldsymbol{\xi}_{p,m}$ is negligible compared with propagation delay $\boldsymbol{\tau}_p$. According to (7) and (8), the following equation could be obtained:

$$\mathbf{A}_{l+1}(\boldsymbol{\tau}, \boldsymbol{\xi}) \approx \mathbf{A}_l(\boldsymbol{\tau}, \boldsymbol{\xi})\mathbf{D}, \tag{17}$$

where $\mathbf{D} = \mathrm{diag}\left(e^{-j2\pi\tau_1\Delta f} \ \ldots \ e^{-j2\pi\tau_P\Delta f} \right)$. Then, $\mathbf{R}_{\mathrm{H}_l}$ could be represented as

$$\begin{aligned}\mathbf{R}_{\mathrm{H}_{l+1}} &= \mathbf{A}_{l+1}(\boldsymbol{\tau}, \boldsymbol{\xi})\mathbf{R}_{\mathrm{B}}\mathbf{A}_{l+1}^{\mathrm{H}}(\boldsymbol{\tau}, \boldsymbol{\xi}) + \sigma^2\mathbf{I} \\ &\approx \mathbf{A}_l(\boldsymbol{\tau}, \boldsymbol{\xi})\mathbf{D}\mathbf{R}_{\mathrm{B}}\mathbf{D}^{\mathrm{H}}\mathbf{A}_l^{\mathrm{H}}(\boldsymbol{\tau}, \boldsymbol{\xi}) + \sigma^2\mathbf{I}.\end{aligned} \tag{18}$$

Then, the key step of smoothing processing calculating the mean of $\mathbf{R}_{\mathrm{H}_l}$, $l = 0, 1, \ldots, L-1$ to get the full-rank covariance matrix is given as

$$\begin{aligned}\widetilde{\mathbf{R}} &= \frac{1}{L}\sum_{l=0}^{L-1}\mathbf{R}_{\mathrm{H}_l}, \\ &= \mathbf{A}_0(\boldsymbol{\tau}, \boldsymbol{\xi})\left(\frac{1}{L}\sum_{l=0}^{L-1}\mathbf{D}^l\mathbf{R}_{\mathrm{B}}\left(\mathbf{D}^l\right)^{\mathrm{H}}\right)\mathbf{A}_0^{\mathrm{H}}(\boldsymbol{\tau}, \boldsymbol{\xi}) + \sigma^2\mathbf{I}, \\ &= \mathbf{A}_0(\boldsymbol{\tau}, \boldsymbol{\xi})\widetilde{\mathbf{R}}_{\mathrm{B}}\mathbf{A}_0^{\mathrm{H}}(\boldsymbol{\tau}, \boldsymbol{\xi}) + \sigma^2\mathbf{I},\end{aligned} \tag{19}$$

where $\widetilde{\mathbf{R}}_{\mathrm{B}} = (1/L)\sum_{l=0}^{L-1}\mathbf{D}^l\mathbf{R}_{\mathrm{B}}(\mathbf{D}^l)^{\mathrm{H}}$.

The next step will focus on proving that if $P \le L$, $\widetilde{\mathbf{R}}_{\mathrm{B}}$ is of full rank. When $\mathrm{rank}(\widetilde{\mathbf{R}}_{\mathrm{B}}) = P$, MUSIC algorithm could be used to conduct processing of $\widetilde{\mathbf{R}}$ though the signals from different paths are coherent with each other.

Firstly, $\widetilde{\mathbf{R}}_{\mathrm{B}}$ could be rewritten as

$$\begin{aligned}\widetilde{\mathbf{R}}_{\mathrm{B}} &= \frac{1}{L}\left[\mathbf{I} \ \ \mathbf{D} \ \ \ldots \ \ \mathbf{D}^{L-1}\right]\begin{bmatrix}\mathbf{R}_{\mathrm{B}} & & \\ & \ddots & \\ & & \mathbf{R}_{\mathrm{B}}\end{bmatrix}\begin{bmatrix}\mathbf{I} \\ \mathbf{D}^{-1} \\ \vdots \\ \mathbf{D}^{1-L}\end{bmatrix}, \\ &= \mathbf{G}\mathbf{G}^{\mathrm{H}},\end{aligned} \tag{20}$$

where $\mathbf{G} = \left[\mathbf{C} \ \ldots \ \mathbf{D}^{L-1}\mathbf{C}\right]$ and $\mathbf{C}\mathbf{C}^{\mathrm{H}} = \mathbf{R}_{\mathrm{B}}/L$.

Obviously, $\mathrm{rank}(\widetilde{\mathbf{R}}_{\mathrm{B}}) = \mathrm{rank}(\mathbf{G})$. As a result, we only need to prove $\mathrm{rank}(\mathbf{G}) = P$. The column permutation of a matrix cannot change its rank, so we have

$$\mathrm{rank}(\mathbf{G}) = \mathrm{rank}\left(\begin{bmatrix}c_{1,1}\mathbf{d}_1 & c_{1,2}\mathbf{d}_1 & \ldots & c_{1,P}\mathbf{d}_1 \\ c_{2,1}\mathbf{d}_2 & c_{2,2}\mathbf{d}_2 & \ldots & c_{2,P}\mathbf{d}_2 \\ \vdots & \vdots & \ddots & \vdots \\ c_{P,1}\mathbf{d}_P & c_{P,2}\mathbf{d}_P & \ldots & c_{P,P}\mathbf{d}_P\end{bmatrix}\right), \tag{21}$$

where $c_{i,j}$ is the i,j-th element of $\mathbf{C}$ and $\mathbf{d}_p = \left[1 \ \ e^{-j2\pi\tau_p\Delta f} \ \ \ldots \ \ e^{-j2\pi\tau_p(L-1)\Delta f}\right]$.

Apparently, as long as there is a nonzero element in each row of matrix $\mathbf{C}$ and the vectors $\{\mathbf{d}_1 \ \ \mathbf{d}_2 \ \ \ldots \ \ \mathbf{d}_P\}$ are linearly independent, $\mathrm{rank}(\mathbf{G}) = P$. Because if all elements in the p-th row of $\mathbf{C}$ are zeros, it means the signal from this path is of no energy, which is unrealistic. Besides, $\{\mathbf{d}_1 \ \ \mathbf{d}_2 \ \ \ldots \ \ \mathbf{d}_P\}$ can form a Vandermonde matrix, which has been proved to be nonsingular. Therefore, $\mathrm{rank}(\widetilde{\mathbf{R}}_{\mathrm{B}}) = \mathrm{rank}(\mathbf{G}) = P$.

After constructing $\widetilde{\mathbf{R}}_{\mathrm{B}}$ with full rank, we can then use the searching method for joint estimation. The spatial spectrum function is

$$P(\boldsymbol{\tau}, \boldsymbol{\theta}) = \frac{1}{\mathbf{A}^{\mathrm{H}}(\boldsymbol{\tau}, \boldsymbol{\theta})\widetilde{\mathbf{U}}_N\widetilde{\mathbf{U}}_N^{\mathrm{H}}\mathbf{A}(\boldsymbol{\tau}, \boldsymbol{\theta})}, \tag{22}$$

in which $\widetilde{\mathbf{U}}_N$ is the noise subspace obtained through the eigenvalue decomposition of $\widetilde{\mathbf{R}}_{\mathrm{B}}$. However, the high computational complexity of the 2D-MUSIC method can greatly increase the cost and limit its practical application. Consequently, we use the TLS-ESPRIT (ESPRIT based on Total Least-Squares) method in this paper for estimating DOA.

3.2. TLS-ESPRIT for DOA Estimation. Define the first $M-1$ rows and the last $M-1$ rows of $\mathbf{A}_0(\boldsymbol{\tau}, \boldsymbol{\xi})$ as $\mathbf{A}_1$ and $\mathbf{A}_2$, which could be seen as the array manifold matrices of these two subarrays. Similarly, $\mathbf{N}_1$ and $\mathbf{N}_2$ are the noise matrices corresponding to $\mathbf{A}_1$ and $\mathbf{A}_2$. Their relationship could be represented as $\mathbf{A}_2 = \mathbf{A}_1\boldsymbol{\Phi}$, and the rotation operator $\boldsymbol{\Phi}$ is

$$\boldsymbol{\Phi} = \mathrm{diag}\left(e^{-j2\pi f_c d\sin\theta_1/c} \ \ldots \ e^{-j2\pi f_c d\sin\theta_P/c} \right). \tag{23}$$

The channel frequency-domain response of two subarrays could be merged into

$$\mathbf{H}' = \begin{bmatrix}\mathbf{A}_1 \\ \mathbf{A}_2\end{bmatrix}\mathbf{B} + \begin{bmatrix}\mathbf{N}_1 \\ \mathbf{N}_2\end{bmatrix} = \overline{\mathbf{A}}\mathbf{B} + \overline{N}. \tag{24}$$

Then, we can get the covariance matrix $\mathbf{R}_{\mathrm{H}'}$ of $\mathbf{H}'$, and the eigenvalue decomposition could be written as

$$\mathbf{R}_{\mathrm{H}'} = \mathbf{E}_{\mathrm{S}}\boldsymbol{\Lambda}_{\mathrm{S}}\mathbf{E}_{\mathrm{S}}^{\mathrm{H}} + \sigma^2\mathbf{E}_N\mathbf{E}_N^{\mathrm{H}}, \tag{25}$$

where $\boldsymbol{\Lambda}_{\mathrm{S}}$ is a diagonal matrix consisting of P bigger eigenvalues of $\mathbf{R}_{\mathbf{H}'}$, while $\mathbf{E}_{\mathrm{S}}$ and $\mathbf{E}_{\mathrm{N}}$ are signal subspace and noise subspace, respectively. According to the equation $\mathrm{rank}(\mathbf{E}_{\mathrm{S}}) = \mathrm{rank}(\overline{\mathbf{A}})$, there is bound to be the unique and full-rank matrix $\mathbf{T}$ with a dimension of $K \times K$, making the following equation tenable:

$$\mathbf{E}_{\mathrm{S}} = \overline{\mathbf{A}}\mathbf{T}. \tag{26}$$

On the basis of ULA's shift-invariance, $\mathbf{E}_{\mathrm{S}}$ could be divided into two parts, $\mathbf{E}_1$ and $\mathbf{E}_2$, corresponding to the two subarrays, which can be represented as

$$\mathbf{E}_S = \begin{bmatrix} \mathbf{E}_1 \\ \mathbf{E}_2 \end{bmatrix} = \begin{bmatrix} \mathbf{A}_1\mathbf{T} \\ \mathbf{A}_1\mathbf{\Phi}\mathbf{T} \end{bmatrix}. \tag{27}$$

From (27), we can get

$$\mathbf{E}_2 = \mathbf{E}_1\mathbf{T}^{-1}\mathbf{\Phi}\mathbf{T} = \mathbf{E}_1\mathbf{\Psi}, \tag{28}$$

where $\mathbf{\Psi} = \mathbf{T}^{-1}\mathbf{\Phi}\mathbf{T}$, meaning that the diagonal elements of $\mathbf{\Phi}$ are the eigenvalues of $\mathbf{\Psi}$. Next, we will try to get $\mathbf{\Psi}$ using the TLS method.

Calculate the product and its eigenvalue decomposition:

$$\begin{bmatrix} \mathbf{E}_1^{\mathrm{H}} \\ \mathbf{E}_2^{\mathrm{H}} \end{bmatrix} \begin{bmatrix} \mathbf{E}_1 & \mathbf{E}_2 \end{bmatrix} = \mathbf{E}\mathbf{\Lambda}\mathbf{E}^{\mathrm{H}}, \tag{29}$$

and then decompose $\mathbf{E}$ into subarrays with the dimension of $K \times K$

$$\mathbf{E} = \begin{bmatrix} \mathbf{E}_{11} & \mathbf{E}_{12} \\ \mathbf{E}_{21} & \mathbf{E}_{22} \end{bmatrix}. \tag{30}$$

We can get $\mathbf{\Psi} = -\mathbf{E}_{12}\mathbf{E}_{22}^{-1}$ and its eigenvalues λ_p, $p = 1, 2, \ldots, P$, which are the diagonal elements of $\mathbf{\Phi}$. So, the estimation of DOA could be obtained as

$$\theta_p = \arcsin\left\{\frac{c \cdot \operatorname{angle}(\lambda_p)}{(2\pi d f_c)}\right\}. \tag{31}$$

3.3. One-Dimensional (1D) Search for Time Delay Estimation. Based on the closed-form estimation of DOA we have obtained using the TLS-ESPRIT method, we can estimate time delays of the signals by one-dimensional (1D) search, where τ_p could be obtained by

$$P(\tau) = \frac{1}{\mathbf{A}^{\mathrm{H}}(\boldsymbol{\tau}, \boldsymbol{\theta}_p)\tilde{\mathbf{U}}_N\tilde{\mathbf{U}}_N^{\mathrm{H}}\mathbf{A}(\boldsymbol{\tau}, \boldsymbol{\theta}_p)}, \quad p = 1, 2, \ldots, P. \tag{32}$$

Besides, if the complex attenuations are independent from each other, then we are not using (32) to estimate time delay considering the array aperture and the estimation accuracy. Also, the improved spatial spectrum function is expressed as

$$P(\tau) = \frac{1}{\mathbf{A}^{\mathrm{H}}(\boldsymbol{\tau}, \boldsymbol{\theta})\mathbf{U}_N\mathbf{U}_N^{\mathrm{H}}\mathbf{A}(\boldsymbol{\tau}, \boldsymbol{\theta})}, \quad p = 1, 2, \ldots, P, \tag{33}$$

where the estimation of time delay τ_p we get from (32) and (33) is corresponding to θ_p, and as a result, the joint estimation of time delay and DOA could be accomplished without extra pairing algorithm.

3.4. Algorithm Steps Conclusion. The whole process of our proposed algorithm could be summarized as the following steps:

(i) Establish the received signal model and get the extended channel frequency-domain response $\mathbf{H}$.

(ii) For coherent signals, use the smoothing processing method and construct the covariance matrix using (19).

(iii) Get the closed-form estimation of DOA by TLS-ESPRIT.

(iv) Get the corresponding estimation of time delay through the 1D researching method. Specifically, when multipath signals are independent, we use an improved searching method expressed as (33), estimating time delay.

4. Analysis of Computational Complexity

In this section, the computational complexities of the proposed method and 2D-MUSIC method are calculated and compared.

For the proposed method, the complexity consists of four parts, constructing the covariance matrix, calculating eigenvalue decomposition, performing TLS-ESPRIT algorithm, and conducting the one-dimensional spectral peak search, the complexities of which are $O(4LNM^2)$, $O(M^3)$, $O(16P^2M)$, and $O(M(M-P)G_\tau)$, with the sum of $O(M^3 + (4LN + G_\tau)M^2 + (16P^2 - PG_\tau)M)$, while for the 2D-MUSIC method, the computational complexity is $O(M^3 + (4LN + G_\tau G_\theta)M^2 - PG_\tau G_\theta M)$, where G_τ and G_θ represent the numbers of search grids regarding time delay and DOA.

As have been discussed in the last chapter, when the complex attenuations are independent from each other, we adopt an improved step for a more accurate time delay estimation. For this improved method, the computational complexity is made up of the calculation of the extended channel frequency-domain response covariance matrix, eigenvalue decomposition, ESPRIT, and the one-dimensional spectral peak search, which are $O(4NM^2L^2)$, $O(M^3L^3)$, $O(16LP^2M)$, and $O(ML(ML-P)G_\tau)$, with the sum of $O(L^3M^3 + (4NL^2 + L^2G_\tau)M^2 + (16LP^2 - LPG_\tau)M)$. Under this condition, the EX-MUSIC method has a computational cost of $O(L^3M^3 + (4NL^2 + L^2G_\tau G_\theta)M^2 - LPG_\tau G_\theta M)$. In this section, $P = 3$, $L = 64$, $M = 8$, and the search range of θ and τ are -180° to 180° and 0 ns to 100 ns. The computational complexities of all methods are shown in Table 1.

Then, the comparison of the complexities is shown in an intuitive way, as can be seen in Figure 2. With the change of N, M, and search step, it could be concluded that 2D-MUSIC and EX-MUSIC have extremely high complexities especially when the search step is small. However, the calculation complexity of the proposed methods is smaller because only 1D (one dimensional) searching is applied for parameter estimation. Compared with the proposed method, our improved method has a higher cost of complexity and can achieve better estimation performance because of the extended frequency response.

5. Simulation Analysis

In this section, simulation experiments are conducted comparing the performance of the proposed method with that of 2-D MUSIC [21]. Furthermore, we have also compared the difference between the improved method and EX-MUSIC when multipaths are independent from each other. To best evaluate the performance of the methods proposed

Table 1: Computational complexity comparison.

Algorithm	Complexity
The proposed method	$O(M^3 + (4LN + G_\tau)M^2 + (16P^2 - PG_\tau)M)$
2D-MUSIC	$O(M^3 + (4LN + G_\tau G_\theta)M^2 - PG_\tau G_\theta M)$
The improved method	$O(L^3M^3 + (4NL^2 + L^2G_\tau)M^2 + (16LP^2 - LPG_\tau)M)$
EX-MUSIC	$O(L^3M^3 + (4NL^2 + L^2G_\tau G_\theta)M^2 - LPG_\tau G_\theta M)$

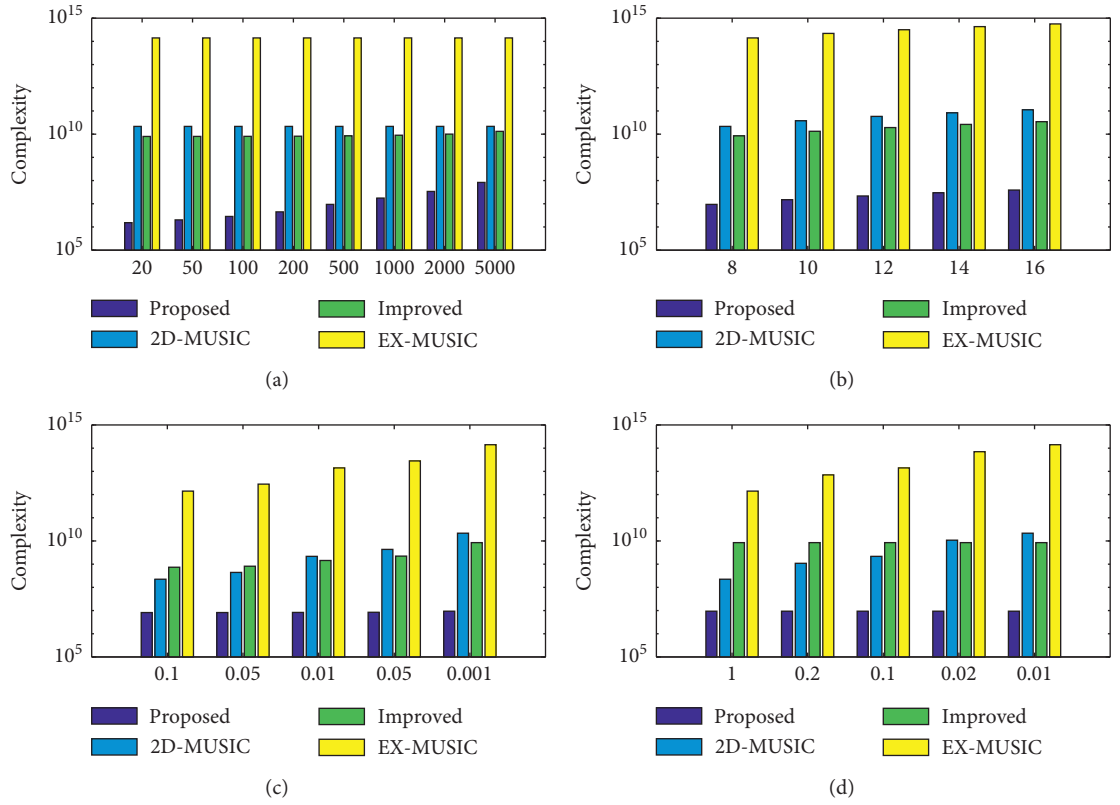

Figure 2: Complexity comparison: (a) change with time intervals when $M = 8$, $\Delta\tau = 0.001$ ns, $\Delta\theta = 0.01^\circ$; (b) change with sensor number when $N = 500$, $\Delta\tau = 0.001$ ns, $\Delta\theta = 0.01^\circ$; (c) change with $\Delta\tau$ when $N = 500$, $M = 8$, $\Delta\theta = 0.01^\circ$; and (d) change with $\Delta\theta$ when $N = 500$, $M = 8$, $\Delta\tau = 0.001$ ns.

in this paper, we choose root mean square error (RMSE) as the measure index using Monte Carlo Simulation. RMSE could be defined as

$$\text{RMSE} = \sqrt{\frac{1}{Q}\sum_{i=1}^{Q}\left\|x - \hat{x}_i\right\|^2}, \tag{34}$$

where Q is the number of Monte Carlo simulation and x and $\hat{x}_i$ represent the i-th actual value and estimated value, respectively. The parameters used in the simulations are set as Table 2.

5.1. Performance of the Proposed Algorithms under Low SNR Conditions. In this part, three conditions are considered to examine the performance of the proposed algorithms by observing the scatter diagrams. The first condition considers three coherent paths whose delays are 3.5 ns, 13.5 ns, and 23.5 ns, and the DOAs of them are -20°, -5°, and 10°, respectively. In the second condition, we suppose the third path is independent from the other two. When solving the problem with coherent signals in condition 1 and condition 2, the proposed method is applied, while in condition 3, all of the three paths are independent and we use the improved method to estimate the parameters.

Table 2: Information about relevant parameters.

Items	Values
Fast Fourier transform period (T_{FFT})	$3.2\,\mu s$
Bandwidth (B)	20 MHz
Carrier frequency (f_c)	2.4 GHz
Element spacing (d)	$c/(2(f_c + B))$

We set $N = 500$, the sensor number $M = 8$, and the number of subcarriers is $L = 64$. There are 100 groups of points plotted for each subfigure. The distribution of estimation under three different conditions is shown in Figure 3. The true values are marked in red.

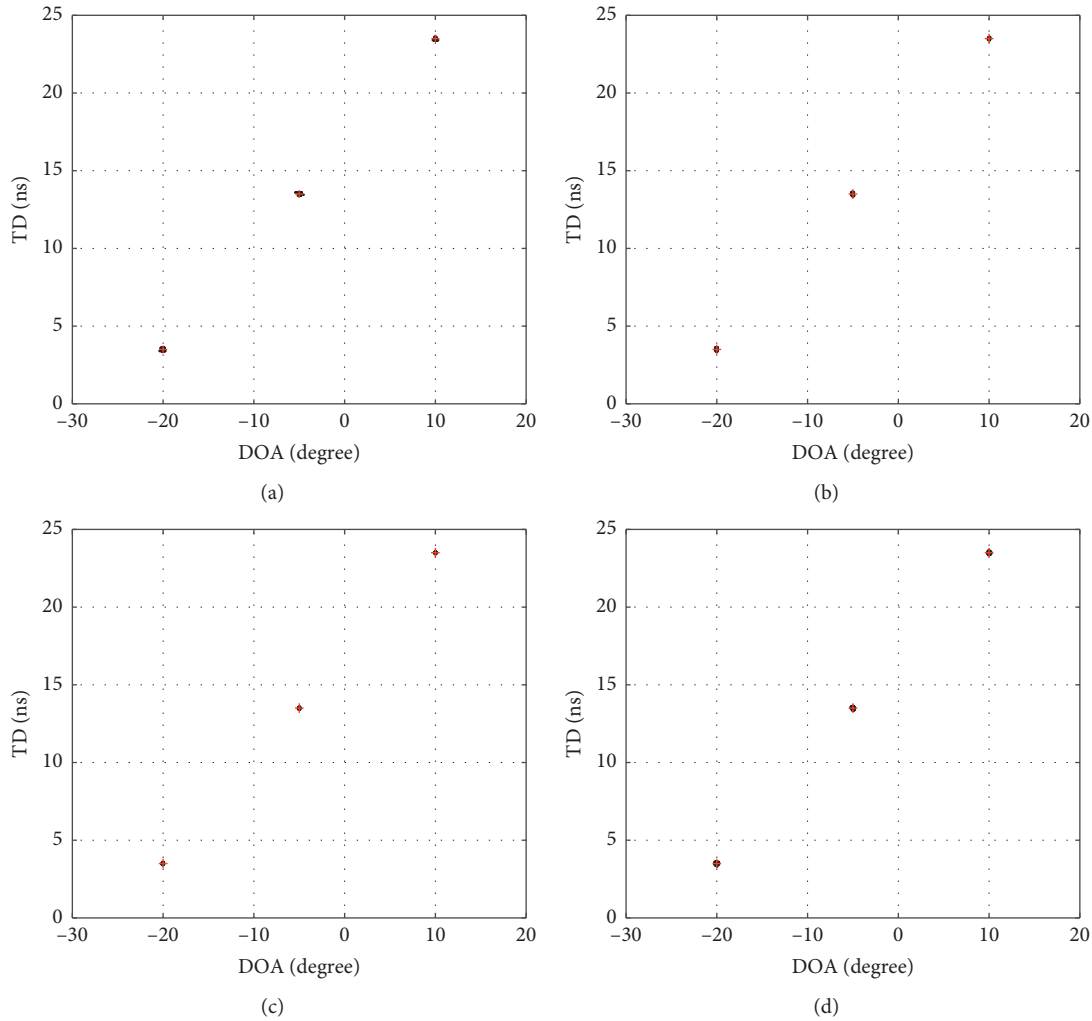

Figure 3: Estimation results distribution under different conditions: (a) condition 1, SNR = −5 dB; (b) condition 2, SNR = −5 dB; (c) condition 3, SNR = −5 dB; and (d) condition 1, SNR = 0 dB.

As can be learned from the following figures, the proposed algorithms can estimate DOAs and time delays successfully under these three conditions, no matter the paths are coherent or not, and more importantly, the results are all concentrated around the actual values, indicating the effectiveness of our proposed algorithm. Besides, the algorithms perform well with low SNR and as a result have strong robustness.

5.2. Performance as SNR Changes. In this simulation experiment, we focus on analyzing the performance of our proposed algorithms in different SNRs. First, the performance of the proposed method is compared with that of 2D-MUSIC [21], the SAGE method in [15], the TOA estimation method introduced in [7], and the DOA estimation method introduced in [12]. The simulation condition is the same as the first condition of Simulation 1 where three paths are coherent. Then, the performance of the improved method is compared with that of EX-MUSIC under the condition that three paths are independent from each other, as described in the third condition of Simulation 1. CRLB used in this subsection is provided by [21]. We set the number of Monte Carlo simulation Q to be 500, and $N = 500$. The sensor number $M = 8$, and the number of subcarriers is $L = 64$. SNR in this simulation ranges from −15 dB to 20 dB at 5 dB intervals, and the performance of the algorithms is shown in Figures 4 and 5.

As can be seen in Figure 4, compared with the traditional TOA and DOA estimation algorithms introduced in [7, 12], the proposed method could greatly improve the accuracy because of the use of smoothing processing. Meanwhile, the improvement of accuracy is at the cost of losing virtual array aperture, and as a result, its performance is not as good as CRLB. Besides, the RMSE performance of the proposed method is better than that of 2D-MUSIC and SAGE, and its computational complexity is much smaller.

Figure 5 shows the comparison of the improved method and EX-MUSIC when all of the paths are independent. The RMSE of the improved method is slightly bigger than that of EX-MUSIC, and the performance of EX-MUSIC is closer to CRLB because the array aperture is expanded in EX-MUSIC.

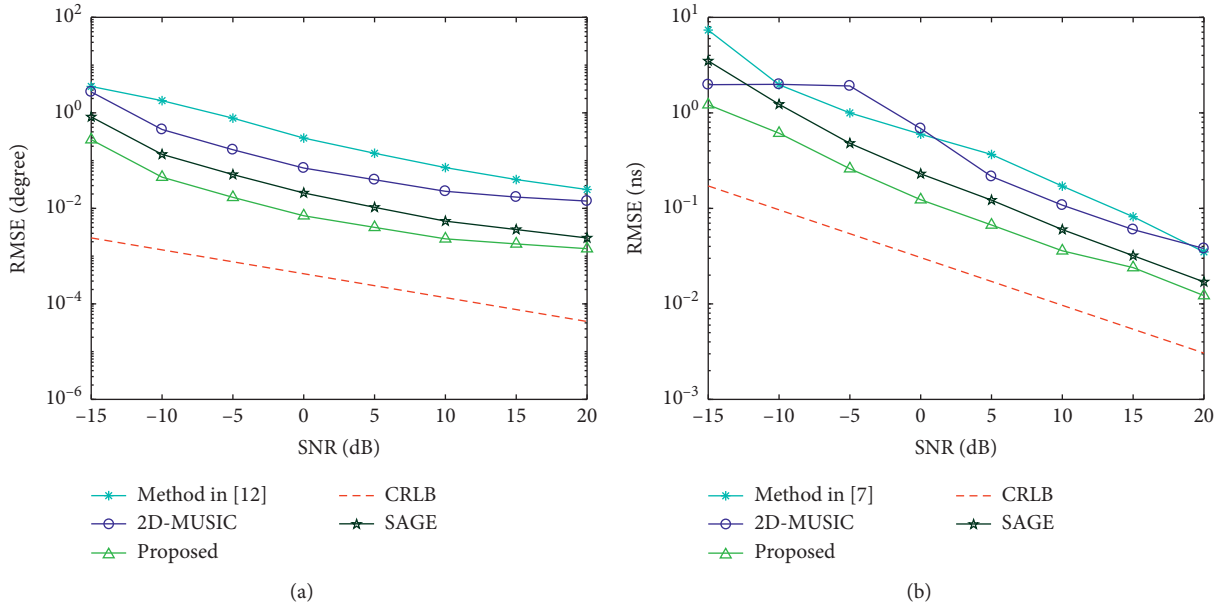

Figure 4: Performance comparison regarding SNR when signals are coherent. (a) DOA and (b) time delay.

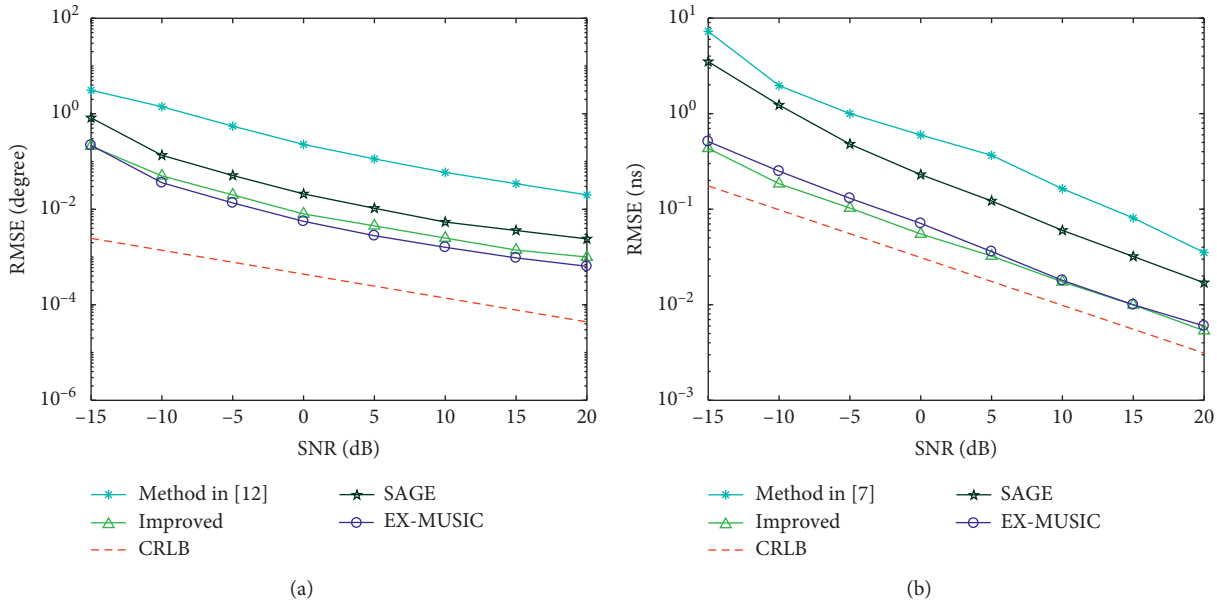

Figure 5: Performance comparison regarding SNR when signals are independent. (a) DOA and (b) time delay.

In addition to expanding the array aperture, using EX-MUSIC also increases the computational complexity. Compared with the proposed method, the improved method has a lower RMSE and also bigger computational complexity, which is still smaller than that of EX-MUSIC. Therefore, our proposed algorithms have better estimation performance than MUSIC-based methods and SAGE.

5.3. Performance as the Number of Time Intervals Changes. In this simulation, the number of time intervals is taken from $N = [20, 50, 100, 200, 500, 1000, 2000, 5000]$, and SNR is set to be 15 dB. Additionally, we set the number of Monte Carlo simulation Q to be 500, the sensor number $M = 8$, and the number of subcarriers is $L = 64$. CRLB used here is provided by [21]. The results are shown in Figures 6 and 7.

RMSE of the algorithms decreases with the increase in the number of time intervals. The performance of our proposed methods is compared with that of 2D-MUSIC [21], the SAGE method in [15], the TOA estimation method introduced in [7], and the DOA estimation method introduced in [12]. As can be seen from Figure 6, with lower computational complexity, the proposed method has smaller RMSE than 2D-MUSIC because of the implementation of

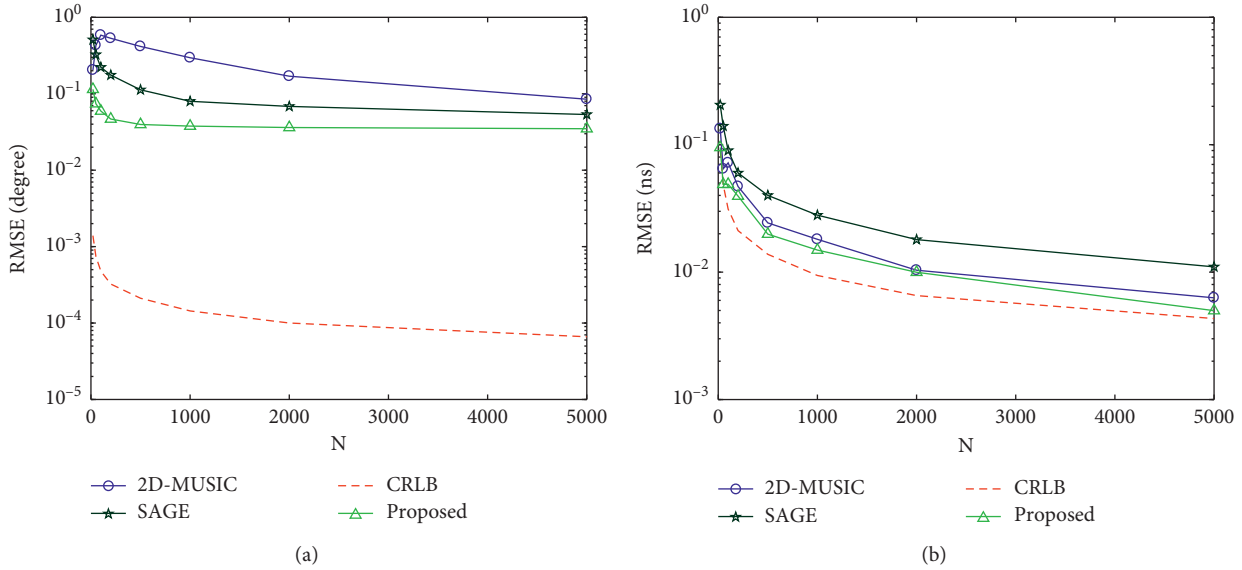

Figure 6: Performance comparison regarding time intervals when signals are coherent. (a) DOA and (b) time delay.

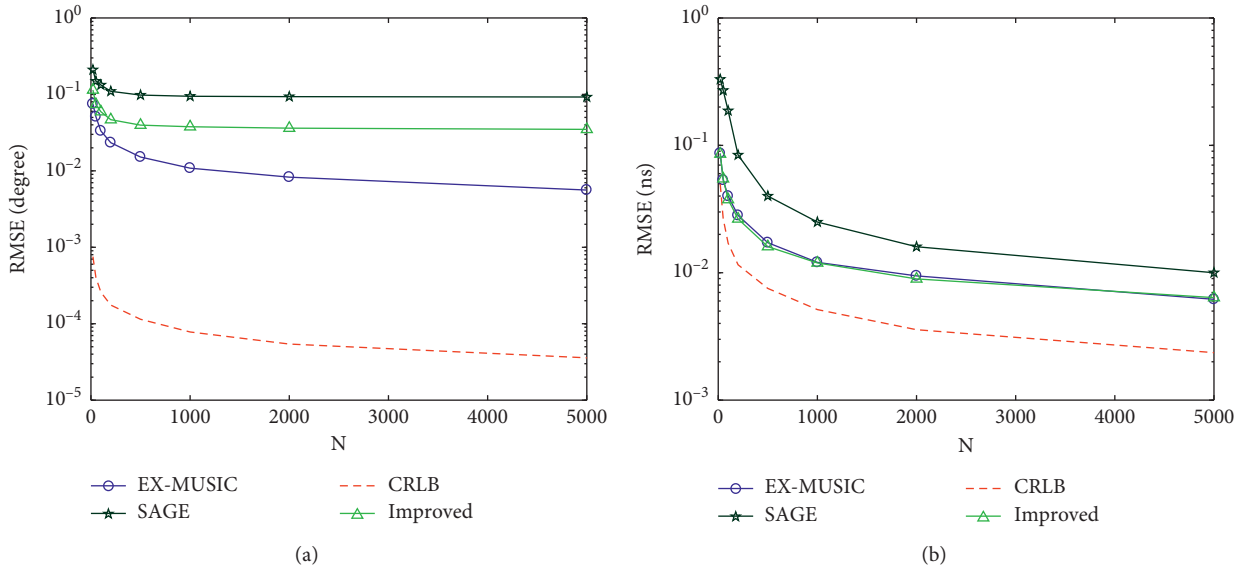

Figure 7: Performance comparison regarding time intervals when signals are independent. (a) DOA and (b) time delay.

smoothing processing when dealing with coherent signals. In addition, it can be concluded that the proposed methods perform better than the traditional TOA and DOA estimation methods. Besides, when signals are independent, the improved method performs nearly the same as the EX-MUSIC method, as can be seen in Figure 7. At this time, independent signals lead to the situation where no information from signal subspace spreads into noise subspace, ensuring the accuracy of the searching method. As a result, EX-MUSIC could perform better due to the expanded array aperture. However, the performance of the improved method is close to that of EX-MUSIC with lower complexity.

6. Conclusions

To achieve the joint DOA and TD estimation of OFDM systems, we propose a joint estimation algorithm used in ULAs that can be applied to complex multipath environments. The channel frequency response of the sensors is extended by using the subcarriers, and as a result, more information is available to estimate the DOA and time delay parameters. Besides, smoothing processing is applied to solve the problem that multipath effect will lead to accuracy loss. Meanwhile, the proposed method is a fast algorithm because TLS-ESPRIT is used in the estimation and its

complexity is smaller than that of 2D-MUSIC. Furthermore, an improved method is proposed as a solution to joint TD and DOA estimation when the paths are independent. In this paper, signal modeling, analysis of computational complexity and simulation experiment are all involved. This paper has provided an effective method that can both improve the estimation accuracy and achieve fast estimation with lower complexity.

Data Availability

The data used to support this study are available within the article.

Conflicts of Interest

The authors declare that they have no conflicts of interest.

Acknowledgments

The work was supported by the National Natural Science Foundation of China (Grant no. 61401513).

References

[1] Z. Rafique, B.-C. Seet, and A. Al-Anbuky, "Performance analysis of cooperative virtual MIMO systems for wireless sensor networks," *Sensors*, vol. 13, no. 6, pp. 7033–7052, 2013.

[2] Y. Y. Wu and W. Y. Zou, "Orthogonal frequency division multiplexing: a multi-carrier modulation scheme," *IEEE Transactions on Consumer Electronics*, vol. 41, no. 3, pp. 392–399, 1995.

[3] C. Knill, F. Roos, B. Schweizer, D. Schindler, and C. Waldschmidt, "Random multiplexing for an MIMO-OFDM radar with compressed sensing-based reconstruction," *IEEE Microwave and Wireless Components Letters*, vol. 29, no. 4, pp. 300–302, 2019.

[4] Z. Mokhtari, M. Sabbaghian, and D. Rui, "A survey on massive MIMO systems in presence of channel and hardware impairments," *Sensors*, vol. 19, no. 1, 2019.

[5] A. Neri, A. Di Nepi, and A. M. Vegni, "DOA and TOA based localization services protocol in IEEE 802.11 networks," *Wireless Personal Communications*, vol. 54, no. 1, pp. 155–168, 2010.

[6] R. Zhang, Y.-H. Quan, S.-Q. Zhu, L. Yang, Y.-C. Li, and M.-D. Xing, "Joint high-resolution range and DOA estimation via MUSIC method based on virtual two-dimensional spatial smoothing for OFDM radar," *International Journal of Antennas and Propagation*, vol. 2018, Article ID 6012426, 9 pages, 2018.

[7] X. Ma, S. Yan, X. Li, and C. Hou, "Super-resolution time delay estimation for narrowband signal," *Iet Radar Sonar Navigation*, vol. 6, no. 8, pp. 781–787, 2012.

[8] H. Jiang, F. Cao, and R. Ding, "Propagator method-based TOA estimation for UWB indoor environment in the presence of correlated fading amplitudes," in *Proceedings of the 2008 4th IEEE International Conference on Circuits and Systems for Communications*, Shanghai, China, May 2008.

[9] D. Oh, S. Kim, S.-H. Yoon, and J.-W. Chong, "Two-dimensional ESPRIT-like shift-invariant TOA estimation algorithm using multi-band chirp signals robust to carrier frequency offset," *IEEE Transactions on Wireless Communications*, vol. 12, no. 7, pp. 3130–3139, 2013.

[10] L. X. Dong, D. M. Wang, B. Ba, and J. H. Wang, "A quasi-cyclic compressed sensing delay estimation algorithm based on progressive edge-growth," *Acta Physica Sinica*, vol. 66, no. 9, Article ID 090703, 2017.

[11] X. D. Leng, B. Ba, Z. Y. Lu, and D. M. Wang, "Sparse reconstruction time delay estimation algorithm based on backtracking filter," *Acta Physica Sinica*, vol. 65, no. 21, Article ID 210701, 2016.

[12] F. C. Cao and M. J. Li, "Frequency domain DOA estimation and tracking of UWB signals," in *Proceedings of the 2010 International Conference on Computational Intelligence and Software Engineering*, Chengdu, China, September 2010.

[13] F.-Q. Wang, X.-F. Zhang, and F. Wang, "Root-MUSIC-based joint TOA and DOA estimation in IR-UWB," *Journal on Communications*, vol. 35, no. 2, pp. 137–145, 2014.

[14] H. Wang, Q. Chang, Y. Xu, and X. Li, "Estimation of interference arrival direction based on a novel space-time conversion music algorithm for GNSS receivers," *Sensors*, vol. 19, no. 11, 2019.

[15] T. Lu, M. Zhang, T. Kang, and A. Zhang, "Joint TOA/DOA estimation using the SAGE algorithm in OFDM systems with virtual carriers," *Journal of Physics Conference Series*, vol. 1169, Article ID 012057, 2019.

[16] M.-C. Hua and H.-C. Liu, "Joint estimation of DOA and TOA for MB-OFDM UWB signals based on frequency-domain processing," *Iet Radar Sonar Navigation*, vol. 10, no. 8, pp. 1337–1346, 2017.

[17] R. Shafin, L. Liu, J. Zhang, and Y.-C. Wu, "Doa estimation and capacity analysis for 3-D millimeter wave massive-MIMO/FD-MIMO OFDM systems," *IEEE Transactions on Wireless Communications*, vol. 15, no. 10, pp. 6963–6978, 2016.

[18] R. Shafin, L. Liu, Y. Li, A. Wang, and J. Zhang, "Angle and delay estimation for 3-D massive MIMO/FD-MIMO systems based on parametric channel modeling," *IEEE Transactions on Wireless Communications*, vol. 16, no. 8, pp. 5370–5383, 2017.

[19] M. C. Vanderveen, C. B. Papadias, and A. Paulraj, "Joint angle and delay estimation (JADE) for multipath signals arriving at an antenna array," *IEEE Communications Letters*, vol. 1, no. 1, pp. 12–14, 2007.

[20] Z. Chen, L. Wang, and M. Zhang, "Virtual antenna array and fractional fourier transform-based TOA estimation for wireless positioning," *Sensors*, vol. 19, no. 3, 2019.

[21] B. Ba and C. Guo, Li Tao, Yu C. Lin, and Yu Wang, Joint for time of arrival and direction of arrival estimation algorithm based on the subspace of extended hadamard product," *Acta Physica Sinica*, vol. 64, no. 7, Article ID 078403, 2015.

[22] Y. Zhu, L. Liu, and J. Zhang, "Joint angle and delay estimation for 2D active broadband MIMO-OFDM systems," in *Proceedings of the 2013 IEEE Global Communications Conference (GLOBECOM)*, Atlanta, GA, USA, December 2013.

[23] L. Chen, W. Qi, E. Yuan, and Y. Zhao, "Joint 2-D DOA and TOA estimation for multipath OFDM signals based on three antennas," *IEEE Communications Letters*, vol. 22, no. 2, pp. 324–327, 2017.

[24] Y. Georgiadou and A. Kleusberg, "On carrier signal multipath effects in relative GPS positioning," *Manuscripta Geodaetica*, vol. 13, no. 3, pp. 172–179, 1988.

[25] M. Navarro and M. Najar, "Frequency domain joint TOA and DOA estimation in IR-UWB," *IEEE Transactions on Wireless Communications*, vol. 10, no. 10, pp. 1–11, 2011.

[26] T- J. Shan, M. Wax, and T. Kailath, "On spatial smoothing for direction-of-arrival estimation of coherent signals," *IEEE Transactions on Acoustics, Speech, and Signal Processing*, vol. 33, no. 4, pp. 806–811, 1985.

[27] C. Zhang and J. Wang, "ES-DPR: A DOA-based method for passive localization in indoor environments," *Sensors*, vol. 19, no. 11, 2019.

[28] H. Xu, Y. Zhang, B. Ba, D. Wang, and X. Li, "Fast joint estimation of time of arrival and angle of arrival in complex multipath environment using OFDM," *IEEE Access*, vol. 6, pp. 60613–60621, 2018.